

Evolution of Microstructure and Magnetic Domains in $\text{Fe}_{74}\text{B}_{20}\text{Nb}_2\text{Hf}_2\text{Si}_2$ Soft Magnetic Alloy Studied by In-Situ Ultra-Rapid Heating TEM and Lorentz TEM Microscopy

P. CZAJA^a AND M. NABIAŁEK^b

^a*The Aleksander Krupkowski Institute of Metallurgy and Materials Science of the Polish Academy of Sciences, 25 Reymonta St., 30-059 Kraków, Poland*

^b*Department of Physics, Faculty of Production Engineering and Materials Technology, Czestochowa University of Technology, al. Armii Krajowej 19, 42-200 Czestochowa, Poland*

Doi: [10.12693/APhysPolA.142.17](https://doi.org/10.12693/APhysPolA.142.17)

*e-mail: p.czaja@imim.pl

The $\text{Fe}_{74}\text{B}_{20}\text{Nb}_2\text{Hf}_2\text{Si}_2$ alloys have been subjected to in-situ transmission electron microscopy ultra-rapid annealing at 900°C. The alloys' microstructure develops into a fine nanocomposite microstructure with a large number of pinning sites, causing the average size reduction of magnetic domains. It is demonstrated that the applied in-situ heating procedure is suited for analysis of the subtle microstructural changes in soft magnetic materials and thus can aid in the optimization of various modes of heat treatment applied for the development of applicable microstructures.

topics: soft magnetic materials, magnetic domains, transmission electron microscopy (TEM)

1. Introduction

The development of modern metallic soft magnetic materials, used in, e.g., motors, sensors, and transformers, has for the past several decades been largely focused on applying annealing heat treatment to metallic glasses in order to produce a fine nanocomposite microstructure [1]. Such a microstructure, comprising minuscule, uniformly distributed precipitates of a magnetic phase within an amorphous matrix, should, in principle, allow simultaneously for high magnetic flux density and low energy core loss. It should thus comply with the random anisotropy model assuming a distribution of magnetic anisotropy axes of the randomly oriented grains and an interplay between the ferromagnetic correlation exchange length and induced anisotropy energies [1]. From the practical point of view, a typically high nucleation density of glass is required in order to ensure a uniform and dense nanocrystalline microstructure. To achieve such conditions annealing treatment can be well performed at different peak temperatures, established based on, e.g., scanning calorimetry measurements. It is commonly found that the onset temperatures may vary depending on the type of annealing and may be higher when conducting rapid annealing lasting for a few seconds.

In conjunction with control over the development of a fine microstructure, special consideration is given to the analysis of a resulting magnetic microstructure, which self-manifests through the distribution and size of magnetic domains responsible for the functional performance of the material. Frequently, Lorentz transmission electron microscopy (L-TEM) is utilised for the analysis of magnetic domain structures [2]. The principles of the contrast mechanism derive from a deflection force experienced by an electron while it travels through the specimen. The deflection force is proportional to both the magnetic induction B and the electron velocity, hence the deflection angle can be determined according to the following formula

$$\theta_L = \frac{e\lambda}{h} B_{\perp} t, \quad (1)$$

where λ is the relativistic electron wavelength, B_{\perp} is the magnetic induction component normal to the electron trajectory, and t is the local specimen thickness [3]. In this contribution, we combine the L-TEM microscopy and the in-situ heating holder based on microelectromechanical systems (MEMS), capable of delivering an instantaneous annealing heat treatment, to monitor and discuss the evolution of magnetic domain structure. More

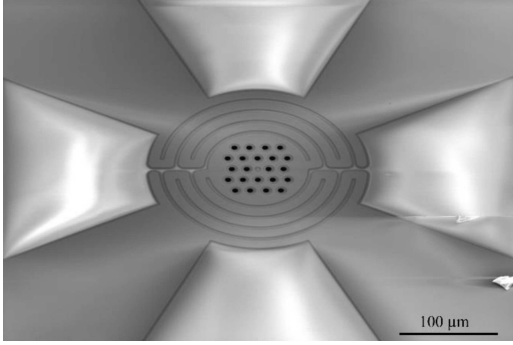


Fig. 1. Scanning electron microscopy image of the heater and grid for lamella deposition on the FEI's NanoExTM-i/v TEM single-tilt heating/biasing holder.

conventional scanning/transmission electron microscopy (STEM) is also employed to trace elemental distribution and phase changes following heat treatment [4, 5].

2. Materials and methods

The alloy with a nominal composition of $\text{Fe}_{74}\text{B}_{20}\text{Nb}_2\text{Hf}_2\text{Si}_2$ [at.%] was prepared from pure elements by suction casting. Thin lamellae for TEM was prepared by focused ion beam (FIB) technique using Thermo-Scientific SCIOS 2 DualBeam. S/TEM and L-TEM analyses were performed by means of Thermo-Scientific Titan Themis x-FEG G3 Cs-corrected S/TEM. The in-situ studies were conducted on the FEI's NanoExTM-i/v TEM single-tilt heating/biasing holder that surpasses more con-

ventional TEM heating holders in terms of precise heat delivery. The traditional heating holders typically utilise a furnace to heat a circa $\varnothing 3$ mm TEM grid sample. The downside of this conventional scenario is that the furnace also heats up most of the holder tip, which results in increased drift and worsened resolution during in-situ experiments. Since the FEI's NanoEx-i/v heating holder is based on a consumable semiconductor MEMS device as the heater, it has a considerably smaller thermal mass, as it is designed to increase heating speed and reduce thermal drift, allowing for rapid acquisition of images even at atomic resolution. The overview of the heater and hollow grid for lamella deposition is shown in Fig. 1. The application of the FEI's NanoEx-i/v heating holder based on a consumable semiconductor (MEMS) device as the heater allowed for analysis of the evolution of microstructure and magnetic domain structure, following ultra-rapid annealing and the subsequent quenching to room temperature. For the experiment, the set point temperature of 900°C was applied, which is above the third peak temperature (878°C) identified for this particular composition by means of differential scanning calorimetry analysis. The microstructure was observed continuously during heating, whereas the L-TEM was performed first at room temperature before heating and subsequently following lamellae quench from 900°C to room temperature.

3. Results

Initially, at room temperature, the lamellae showed some degree of crystallinity as inferred from the bright field image (BF) presented in Fig. 2a.

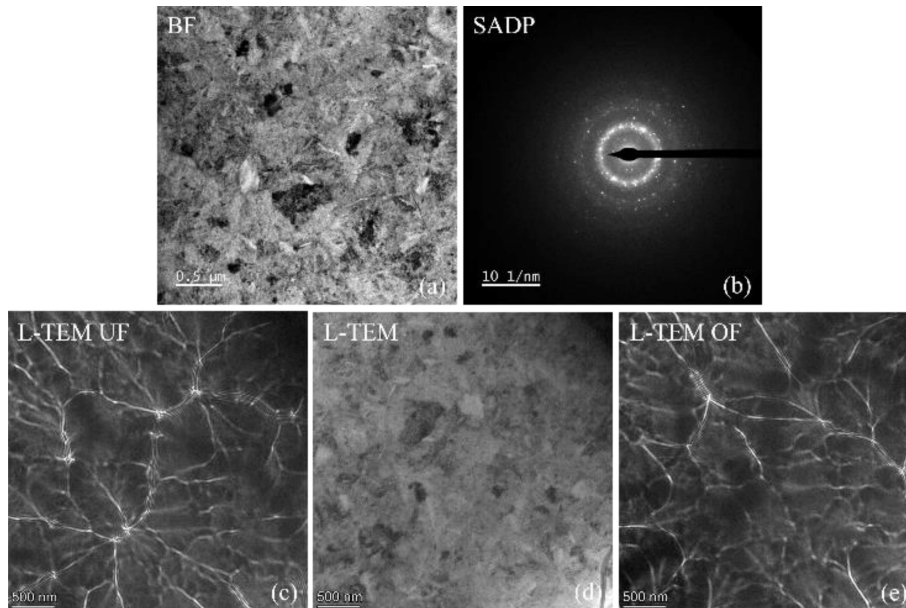


Fig. 2. Bright field image (a) and the corresponding selected area electron diffraction pattern (b) together with L-TEM images (c, d) taken at room temperature from the as prepared thin lamella of the $\text{Fe}_{74}\text{B}_{20}\text{Nb}_2\text{Hf}_2\text{Si}_2$ alloy. The acronyms UF and OF indicate under and over focus conditions, respectively.

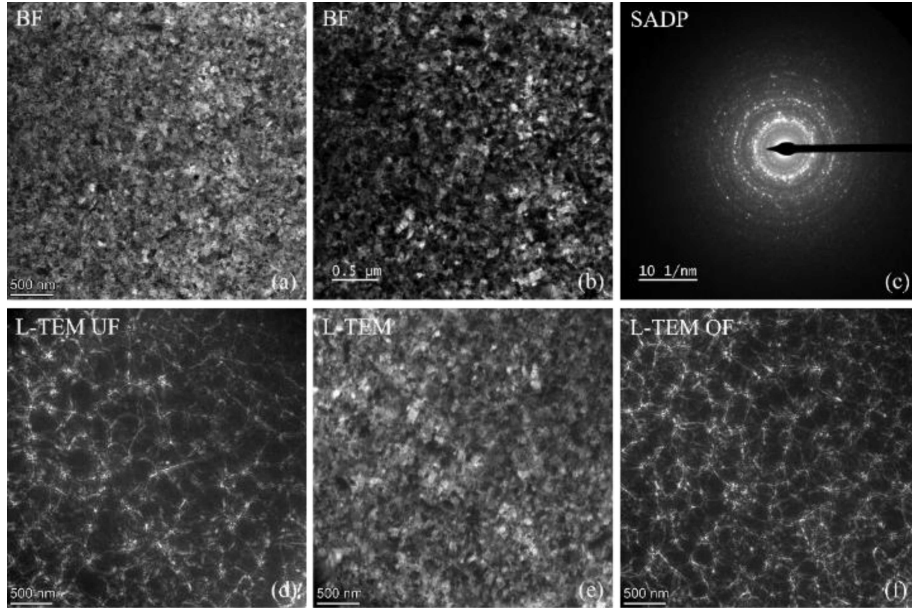


Fig. 3. Bright field images (a, b) and the corresponding selected area electron diffraction pattern (c) together with L-TEM images (d–f) taken at room temperature from the thin lamella of the $Fe_{74}B_{20}Nb_2Hf_2Si_2$ alloy following heat treatment at $900^{\circ}C$. The acronyms UF and OF indicate under and over focus conditions, respectively.

The BF image shows diffraction contrast and, in addition to that, a few dendritic-like features also can be well detected on the image. It is in accordance with the corresponding selected area electron diffraction pattern (SAED) shown in Fig. 2b. It demonstrates a diffused ring-like pattern typical for nanocrystalline materials. This was somewhat surprising since, in addition to that, a few dendritic-like features also can be well detected on the image. It is in accordance with the corresponding selected area electron diffraction pattern (SAED) shown in Fig. 2b. It demonstrates a diffused ring-like pattern typical for nanocrystalline materials. This was somewhat surprising since, in the initial state following FIB preparation and lamellae extraction, the lamellae were clearly in an amorphous state, which has been verified by TEM. It can thus be assumed that the crystallization has taken place to some extent in the initially amorphous sample, most likely during the mounting process of the lamellae to the MEMS grid, accomplished with Pt GIS. Nonetheless, the microstructure was not fully developed. Following microstructure analysis, L-TEM was performed to assess the size and distribution of magnetic domains. The Lorentz microscopy images were obtained in the Fresnel mode, under in-focus, under focus (UF) and over-focus (OF) conditions. The results are illustrated in Fig. 2c–e. The magnetic domain walls are well visible through white and black lines, which reverse contrast depending on the focus conditions. In general, the domains found are large, and only a few pinning sites can be noted. This indicates a low coercivity and a high saturation magnetization in the alloy.

Following ultra-rapid heat treatment performed in situ with the aid of the FEI's NanoExTM-i/v holder, the microstructure develops into a fine nanocrystalline microstructure with nanometre-sized grains (Fig. 3a and b). The corresponding SADP (Fig. 2c) is again a ring pattern but this time more intense, and it can be well indexed according to the α -Fe and $Fe_{23}B_6$ phases, which is consistent with the literature. The L-TEM analysis, given again as a series of UF, OV and in-focus images in Fig. 2d–f, reveals that the average domain size decreased substantially. A larger number of pinning sites associated with grain boundaries can be detected on the images [6]. This may suggest more hard magnetic properties as compared to the initial alloy state [7].

Aside from nucleation and grain growth, some changes in the elemental distribution following heat treatment were also exposed. The chemical composition analysis was conducted by STEM with energy-dispersive X-ray spectroscopy (STEM-EDX). The example results are shown in Fig. 4. Figure 4a presents the high-angle annular dark-field STEM (STEM-HAADF) image and is accompanied by elemental distribution maps for each given element (Fig. 4b–f). A distinct phase contrast indicating precipitation and/or segregation appears already on the STEM-HAADF image. The dark contrast areas, when confronted with elemental distribution maps, correspond to areas enriched in Hf and Si and leaner in Fe as opposed to bright contrast areas, which in principle are richer in Fe and poorer in Hf and Si. Thus these three elements are primarily subject to local concentration fluctuations.

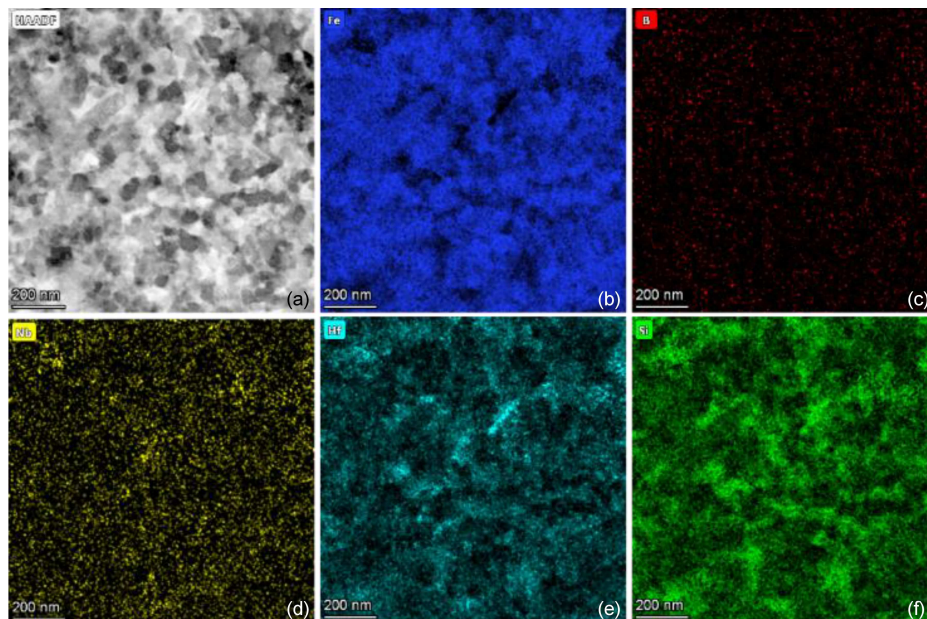


Fig. 4. STEM image (a) and the corresponding elemental distribution maps (b–f) taken at room temperature from the $\text{Fe}_{74}\text{B}_{20}\text{Nb}_2\text{Hf}_2\text{Si}_2$ alloy thin lamella following heat treatment at 900°C .

More quantitatively, the EDX analysis allowed for the identification of the following phase compositions, i.e., (i) Fe-rich $\text{Fe}_{75.6}\text{Nb}_{1.9}\text{Hf}_{4.8}\text{Si}_{17.8}$ at.% and (ii) Hf- and Si-rich $\text{Fe}_{47}\text{Nb}_{1.9}\text{Hf}_{12.5}\text{Si}_{38.6}$ at.% phases.

4. Conclusions

Ultra-rapid annealing has been applied to a thin lamella of the $\text{Fe}_{74}\text{B}_{20}\text{Nb}_2\text{Hf}_2\text{Si}_2$ alloy. The microstructure of the alloy undergoes profound refinement from a nearly amorphous state to a nanocrystalline state. Phase segregation is noted, and it primarily concerns the change in the elemental distribution of Fe, Hf and Si. Microstructure changes cause the initially large magnetic domains to shrink in size due to the development of a large number of pinning sites associated with grain boundaries.

Acknowledgments

The Aleksander Krupkowski Institute of Metallurgy and Materials Science of the Polish Academy of Sciences is gratefully acknowledged for supporting this study.

References

- [1] G. Herzer, *Acta Mater.* **61**, 718 (2013).
- [2] A. Kovacs, K.G. Pradeep, G. Herzer, D. Raabe, R.E. Dunin-Borkowski, *AIP Adv.* **6**, 056501 (2016).
- [3] J.N. Chapman, *J. Phys. D: Appl. Phys.* **17**, 623 (1984).
- [4] J. Long, Y. Qin, T. Nuhfer, M. De. Graef, D.E. Laughlin, M.E. McHenry, *J. Appl. Phys.* **101**, 09N115 (2007).
- [5] F. Hosseini-Nasb, A. Beitollahi, M.K. Moravvej-Farshi, *J. Magn. Magn. Mater.* **373**, 255 (2015).
- [6] Z. Akase, S. Aizawa, D. Shindo, P. Sharma, A. Makino, *J. Magn. Magn. Mater.* **375**, 10 (2015).
- [7] P. Sharma, X. Zhang, Y. Zhang, A. Makino, *Scripta Mater.* **95**, 3 (2015).